Bulgarian Journal of Physics vol. **48** (2021) 645–654

# Shapes and symmetries in $A \sim 130$ nuclei: A Perspective through Measured Transition Probabilities

**P. Das, U. Lamani, H.K. Singh**

Physics Department, Indian Institute of Technology Bombay, Powai, Mumbai-400076, India

Received *31 October 2021*

**Abstract.** We investigated two isotones ($N = 74$) – $^{129}$Cs and $^{127}$I in the mass region 130 – both with moderate deformation, exhibiting signature splitting in their positive-parity bands based on the $\pi g_{7/2}$ configuration. Interestingly, signature inversion occurs in $^{127}$I at low spin ($19/2^+$), while no inversion has been observed for $^{129}$Cs. Here we present some new results on the reduced transition probability B(E2) for states belonging to $^{127}$I. The lifetimes in picoseconds were measured using the Doppler Shift Attenuation Method (DSAM). We utilized the single quasi-particle rotor model to theoretically describe our results, which suggest higher deformation and triaxiality ($\varepsilon_2 = 0.23$, $\gamma = 28^\circ$ in Lund convention) for $^{127}$I than for $^{129}$Cs ($\varepsilon_2 = 0.15$, $\gamma = 18^\circ$).

KEY WORDS: Doppler Shift Attenuation Method, mass region 130, particle rotor model, reduced transition probability, signature splitting.

## 1 Introduction

Various nuclear shapes such as prolate, oblate or triaxial – with underlying symmetries and associated conserved quantities – have drawn considerable interest during recent years. In the mass region $\sim 130$, nuclei exhibit various nuclear phenomena such as signature splitting and inversion, backbending, decoupled band, chirality [1–4]. Signature splitting has been studied extensively [5], but there is no unique mechanism for signature inversion which is well established and conclusive. Two distinct signature partner bands with $\Delta I = 2$ appear in the decay scheme, and are energetically favored and unfavored. Favored energy states have less energy than unfavored ones, leading to "normal" signature splitting. However, in some cases, the phenomenon is reversed, known as "anomalous" signature splitting. Anomalous (normal) signature splitting gets flipped to normal (anomalous) splitting at a critical spin, known as signature inversion. It has been our interest to observe which way the flipping occurs and to understand the underlying physics.

The reduced transition probabilities B(M1) and B(E2) are the critical observables, obtained from the measured lifetimes, to describe the nuclear wavefunc-

tion accurately. Doppler Shift Attenuation Method (DSAM) is a sophisticated and accurate technique to measure lifetimes in ps-fs range. In an earlier work, we investigated the odd-odd nucleus $^{126}$I [6, 7] – a triaxial nucleus with changing shape and axis of rotation when excited to high angular momentum states – which exhibited both signature splitting and inversion. Among the odd-even isotones (N=74), we recently studied $^{129}$Cs [8] and $^{127}$I nuclei, both showing signature splitting. Interestingly, signature inversion happens at a low spin $19/2^+$ for $^{127}$I, but not observed for $^{129}$Cs till the observed high spins [8]. We compared their signature splitting, inversion and B(E2) values with the theoretical particle rotor model (PRM) estimates, and extracted the nuclear deformation parameters ($\varepsilon_2$, $\gamma$ in Lund convention). Here our focus is to investigate the observed behavior in $^{127}$I for the positive-parity band in the light of new results on B(E2). We confirmed this band to be based on the valence proton configuration $\pi g_{7/2}$, with a larger shape asymmetry ($\varepsilon_2 = 0.23$, $\gamma = 28^\circ$) than for $^{129}$Cs ($\varepsilon_2 = 0.15$, $\gamma = 18^\circ$) [8].

## 2 Material and Methods

### 2.1 Doppler shift attenuation method

The Doppler shift in $\gamma$-rays emitted from recoiling nuclei, as observed in the laboratory frame, within the first-order approximation for $\beta \ll 1$, can be expressed as [9]:

$$E_\gamma = E_\gamma^0(1 + \beta\cos\theta), \tag{1}$$

where $E_\gamma$ is the shifted $\gamma$-ray energy, $E_\gamma^0$ is its actual energy, $\beta = v/c$ is the recoil velocity, and $\theta$ is the angle between the detector and beam axis. The continuous deceleration of recoil nuclei in the stopping medium leads to a statistically skewed Gaussian profile in the low (high)-energy side of the actual $\gamma$-ray peak depending on the obtuse (acute) value of $\theta$. From these skewed Gaussian profiles (lineshapes), the lifetime values are determined using the DSAM.

Figure 1, part (i) presents the position and shape of the measured $\gamma$-peak, when the lifetime of a decaying state is compared with the stopping time of the recoils in a given medium. The part (ii) of the figure gives a typical arrangement of detectors in the forward, backward, and normal to the beam direction. Three different scenarios for measuring lifetimes exist. (a) For the states with very short lifetimes and feeding times, the velocity distribution of nuclei is narrow, and all $\gamma$-rays associated with these levels are emitted before the complete stopping of the nuclei. The resulting spectrum shows a complete shift of the peak energy (fully Doppler-shifted transitions). (b) The lifetimes and feeding times are within the range of the stopping time scale of the recoiling nuclei in the backing (or stopper) – and the associated peaks in the spectrum show distinct Doppler-shifted peaks (lineshapes) – corresponding to the gamma-ray intensity distribution between energies corresponding to the stopped and full ve-

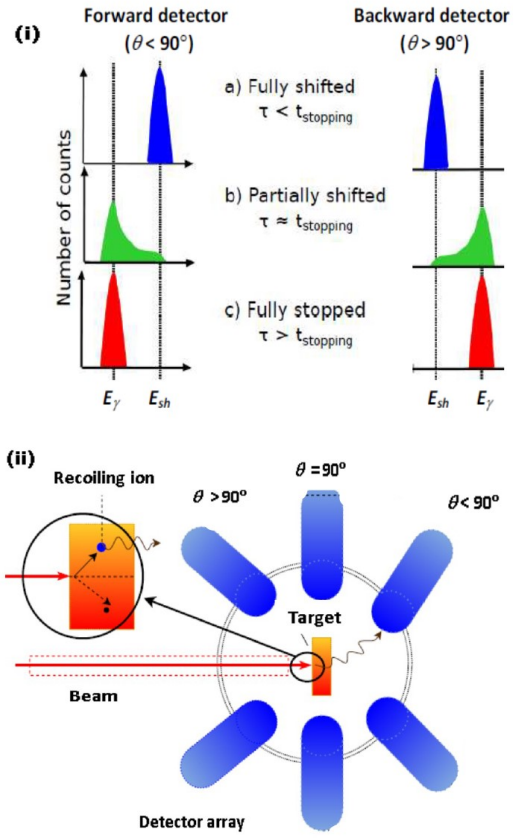


Figure 1. (Color online) (i) Position and shape of the $\gamma$-ray peak decaying from a nuclear state with lifetime in three different ranges, when compared with the stopping time of moving recoils in a medium. (ii) A typical arrangement of detectors in the DSAM measurement.

locity components. (c) For states with long lifetimes or long feeding times, all associated gamma-rays show no Doppler shift, as the emission of these transitions occurs after the nucleus has come to rest in the stopping material. It is noteworthy that the stopping material can be the target itself, as in our present and earlier studies [7, 8]. It can also be a different high-Z material like gold. In case (a), the lifetime of the states is obtained by the centroid shift method [9]. In case (b), the lifetime can be obtained by comparing the gamma-ray lineshapes at various angles other than 90°, with theoretically calculated lineshapes. This was the case of DSAM employed in our study.

## 2.2 Experimental details

We performed two experiments with (i) $^{7}$Li ($E_{\text{beam}} = 50$ MeV) on $^{124}$Sn target, and (ii) $^{11}$B ($E_{\text{beam}} = 70$ MeV) on $^{124}$Sn target, using the 14 MV Pelletron accelerators at the Inter University accelerator center (New Delhi, India) and the Tata Institute of Fundamental Research (Mumbai, India), respectively. The INGA set-ups [10, 11] consisting of 15-18 Compton suppressed HPGe clover detectors, were utilized for the detection of $\gamma$-rays. The details of the two experimental set-ups are very similar. So, we only describe the first experiment as it produced the high spin states of $^{127}$I via a 4n channel, providing the new lifetime results. With the second reaction, we studied $^{129}$Cs [8] and some of those results are also presented and discussed here.

We utilized an enriched (99.4%) $^{124}$Sn self-supporting target of thickness $\sim 2.7$ ($\pm 0.1$) mg/cm$^2$ [7], that acted additionally as the stopper. The target foil of uniform thickness was carefully prepared by rolling method, and its thickness was determined by weighing and finding its area accurately. At 50 MeV of beam energy, the residues acquired the average recoil velocity of 0.67% of speed of light. The list mode data were collected for two- and higher-fold gamma coincidences. The data were calibrated 0.5 keV/Channel using the radioactive sources $^{152}$Eu and $^{133}$Ba. Further details of the experiments and data sorting can be found in our earlier works [7, 8].

## 2.3 Data analysis

We analyzed the Doppler lineshapes using three asymmetric matrices: 32° vs all detectors to observe forward Doppler shift, 148° vs all detectors to observe backward shift, and 90° (normal) vs all detectors to examine the nearby gamma-peaks as contaminants. We employed two gating procedures, Gating on Transition Above (GTA) and Gating on Transition Below (GTB) [7, 8, 12]. The GTB analysis has the advantage of good statistics of data, which yields a good accuracy of the results; GTA data is less contaminated and free from parameters due to side-feedings, but typically suffers poor statistics. In both gating techniques, we included the gates on the shifted and unshifted components of the $\gamma$-transition. Finding lifetimes in two independent ways (GTA and GTB) improves the certainty of results. A symmetric $E_\gamma$- $E_\gamma$ matrix was utilized to find the gamma-ray intensities for the branching ratios and side-feeding contribution. Figure 2 presents the partial decay scheme of $^{127}$I. We present here the lifetimes of three levels (in blue) marked with "$*$".

Figure 3 presents an example of the experimental spectra fitted using the LINESHAPE program of J.C. Wells [13]. In DSAM, the Monte Carlo technique is utilized to generate lineshapes. There are two computer programs – DECHIST and HISTAVER. The program DECHIST simulates the time-dependent velocity profile in the target/backing medium corresponding to the given time step for

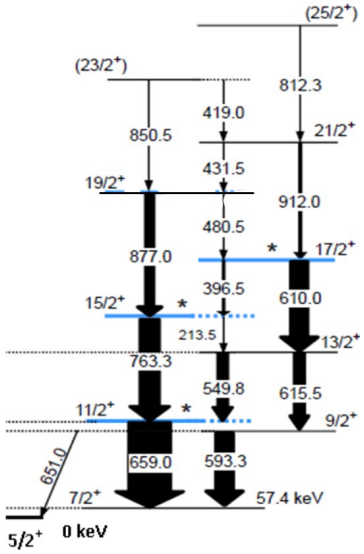


Figure 2. (Color online) Partial decay scheme of $^{127}$I showing the yrast positive-parity band with levels (in blue) and starred ($*$) for new measured lifetimes using DSAM.

all the simulated recoils. The HISTAVER program uses this time-dependent velocity profile convoluted with the detector angle. Apart from the detector angle, the program needs the detector size and its distance from the target to estimate

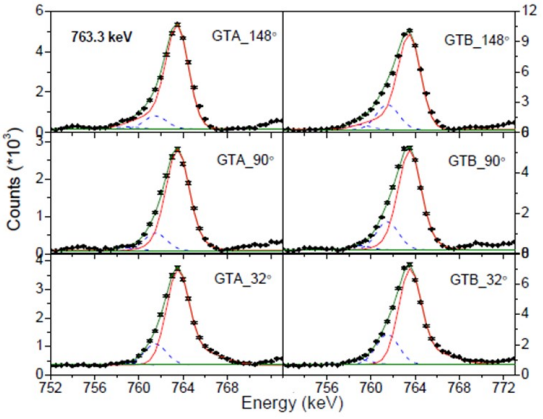


Figure 3. (Color online) Lineshapes of the 763.3 keV $\gamma$-transition decaying from the state $15/2^+$ for the Gating on transition above (GTA) and Gating on transition below (GTB) analyses in DSAM. The fitting in red is the DSAM lineshape, in blue (dashed) is the contaminant peak, and in black is the overall profile.

the solid angle. The efficiency of the detector was also required. Two crucial inputs to the program are the branching ratios and side-feeding intensities, determined from the measured $\gamma$-transitions. We also incorporated the Doppler broadening [7, 8] for the $\gamma$-peaks in finding the accurate intensities.

Another important parameter is the side-feeding lifetimes ($\tau_{\text{sf}}$), and its initial value was estimated using the computer program COMPA [14]. An empirical relation (Eq. 2) depends on the entry state energy ($E_{\text{entry}}$ (MeV)) and the level energy ($E_{\text{lev}}$) for each spin ($I_{\text{lev}}$), and on the maximum angular momentum attained $I_{\max} = 36\hbar$ for our studied reaction [7]).

$$\tau_{\text{sf}}(E_{\text{lev}}, I_{\text{lev}}) \sim 0.007(E_{\text{entry}}(I_{\text{lev}}) - E_{\text{lev}}) + 0.007(I_{\max} - I_{\text{lev}}). \quad (2)$$

At first, we carried out the analysis by gating on below transition (GTB) of interest. We tried to obtain consistent results using two different models of side-feeding for the GTB analysis. The first model was a rotational model of a five-level cascade of constant dynamic moment of inertia and the second was a two-level model. For the latter, we fixed the lifetime for one level during fitting to the value estimated from the empirical relation (Eq. 2), while varying the lifetime of other level. Both models provide a sound understanding of the side-feeding lifetimes. However, it is often desirable to avoid side-feeding contributions to minimize the error in results. Hence, we adopted the procedure of gating on the above transitions (GTA) also. The major limitation of GTA was the low intensities of $\gamma$-peaks as compared to those observed in GTB. To improve $\gamma$-ray intensities, we used summed gated spectra to get the Doppler-shifted profiles. Finally, we carried out simultaneous three-angle and cascade fitting starting from the top to bottom levels. So far, we have found the confirmed results for three states $17/2^+$, $15/2^+$, and $11/2^+$.

### 2.4 Theoretical calculation

We utilized the single quasi-particle rotor model (PRM) [15] – a hydrodynamical model, also called the irrotational flow (IRF) model – to study nuclear behavior in $^{127}$I. The computer code was procured from I. Ragnarsson [16]. Although theoretical results for the odd-mass iodine isotopes existed in the literature [17], our interest was to reproduce simultaneously the signature splitting and its inversion along with the new experimental results on reduced transition probabilities. The important inputs to the program were the single-particle orbits for the quasi-particle, the deformation parameters of the core ($\varepsilon_2$, $\varepsilon_4$, $\gamma$), and the moment of inertia parameters. The variable moment of inertia parameters were defined as A00 [$\equiv 1/(2J_0)$] and Stiff [$\equiv 1/(2J_1)$] in the Harris expansion, $\Im_0 = J_0 + J_1\omega^2$, where $\omega$ is the rotational frequency. We used the values for the neighboring even-even nucleus $^{128}$Xe [18] ($J_0 = 17.0$ MeV$^{-1}\hbar^2$ and $J1 = 25.0$ MeV$^{-3}\hbar^4$).

## 3 Results and Discussion

A detailed spectroscopic investigation was carried out by Ding *et al.* [19], but without any lifetime measurement. We have determined the level lifetimes by fitting the Doppler lineshapes as described earlier. Our initial results for the states $17/2^+$, $15/2^+$ and $11/2^+$ decaying via the intense transitions, 610.0 keV, 763.3 keV and 659.0 keV are $1.34^{+0.17}_{-0.20}$ ps, $0.79^{+0.06}_{-0.09}$ ps, and $1.42^{+0.10}_{-0.11}$ ps, respectively. The error in the lifetime values was estimated by finding how the $\chi^2$ got affected by changing the lifetime values using the MINOS subroutine of the LINESHAPE software package [13]. Finally, we arrived at the error value when the $\chi^2$ increased by 1. This way, the error could be symmetric or asymmetric around the lifetime value depending upon the neck of the parabola. The total systematic error – including the uncertainties in target thickness (5%), stopping power values (5%) [20], continuous production and stopping of the recoils in the target ($< 5\%$), and estimation of recoils flying in vacuum ($< 5\%$) – could at the most be 15% which is not included in the quoted error values.

The B(E2) values were estimated [7] using Eq. (3)

$$B(E2) = \frac{0.0816 f_\gamma(E2)}{E_\gamma^5(E2)[1+\alpha_t(E2)]\tau}[(eb)^2], \tag{3}$$

where $f_\gamma$, $\alpha_t$ are the branching ratio, total internal coefficient, respectively; $\tau$ is the measured lifetime in ps, and $E_\gamma$ is the $\gamma$-ray energy in MeV. The values of $\alpha_t$ were considered zero because of reasonably high energies of the $\gamma$-transitions ($E_\gamma \geq 100$ keV). Moreover, the mixing from higher multipole is negligible for the stretched E2 transitions. The error in B(E2) was determined by the error propagation method. Figure 4 presents the results for the mentioned positive-parity states, in comparison with the theoretical values estimated using the PRM calculation. The theoretical estimates were within the range of experimental values.

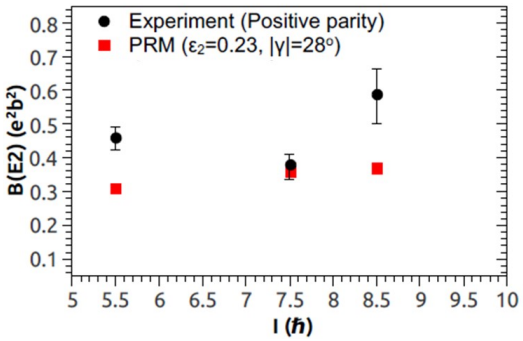


Figure 4. (Color online) The B(E2) values obtained from the measured lifetimes of states belonging to the yrast positive-parity band in $^{127}$I.

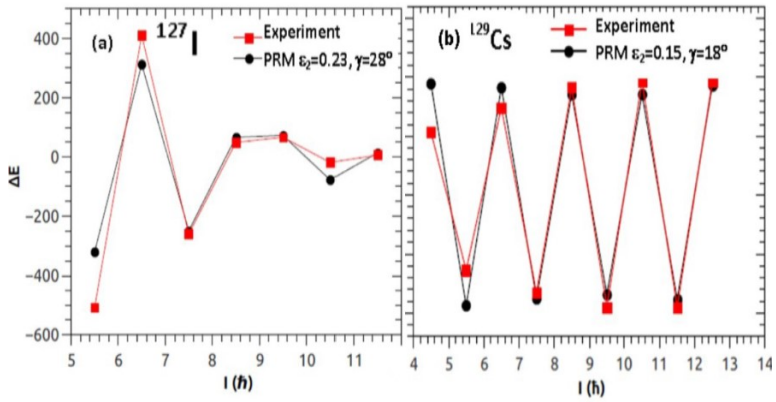


Figure 5. (Color online) A comparison of the signature splitting behavior for the yrast positive parity bands in (a) $^{127}$I , and (b) $^{129}$Cs, with the estimates from the particle rotor model.

Figure 5 shows a comparison of signature splitting for the two N=74 isotones, $^{129}$Cs [8] and $^{127}$I, for their positive-parity bands. There is a similarity in both plots that the energy for $11/2^+$ is lower than that for the $13/2^+$ state, i.e. the same signature bands are favored near just above the bandhead. A stark difference is also noticeable that there is signature inversion for $^{127}$I at around $19/2^+$, but $^{129}$Cs same splitting continues without inversion till the highest spin observed.

We utilized different set of values of deformation parameters $\varepsilon_2$ and $\gamma$ to simultaneously match the signature splitting and B(E2) values. The best agreement was obtained for $\varepsilon_2 = 0.23$ and $\gamma = 28^\circ$ (Figures 4 and 5(a)). In fact, the splitting was sensitively dependent on the $\gamma$ value, and B(E2) on $\varepsilon_2$ values. So, fixing their values uniquely was possible. On the other hand, $^{129}$Cs is comparatively much less deformed (Figure 5(b)). To describe the inversion in $^{127}$I with an increase in the value of B(E2) at $17/2^+$ (Figure 4), we would need to further increase the value of $\gamma$ keeping the same $\varepsilon_2$ value. For the valence particle configuration near the bandhead, the estimated probabilities from PRM for various orbitals are – 75% for $g_{7/2}$, 5% for $d_{5/2}$, and 20% for others ($s_{1/2}$ and $d_{3/2}$).

In the Cranking model picture, the favored states corresponds to signature $\alpha$=-1/2 with *j*=7/2 – for the valence single quasi-particle $\pi g_{7/2}$ as predominant configuration – considering the definition of $\alpha = (1/2)(-1)^{(j-1/2)}$. We indeed observed normal signature splitting in $^{129}$Cs (Figure 5(b)), because states 11/2, 15/2, 19/2 ... are lower in energy than the other signature ($\alpha$=+1/2) states 9/2, 13/2, 17/2 ... However, for $^{127}$I the sequence starts with normal splitting, but inverts to anomalous splitting at $19/2^+$ (Figure 5(a)). Since the Cranking picture is more accurate at very high spins than low spin states, we conjecture that another inversion may occur in $^{127}$I at an higher spin than observed ones, so that the normal splitting is restored. Another feature we can infer from the observed

decay scheme of $^{127}$I (Figure 2) is that a significant amount of decoupling [21] happens. The decoupling parameter is likely to be within $0.5 <\mid a \mid< 1$ as apparent from the closeness of the energy states $9/2^+$ and $11/2^+$. But the spins are still in the increasing order, so the possibility of $\mid a \mid> 1$ is ruled out.

## 4 Conclusions

We have investigated the behavior of signature splitting for the yrast positive-parity band belonging to $^{127}$I in comparison to another $N = 74$ isotone $^{129}$Cs. The B(E2) values derived from the lifetime measurement lie between 0.15 to 0.6 $(eb)^2$. This report presents the new lifetime results for three states in the range of 0.8 to 1.4 ps. For $^{127}$I, the deformation parameters ($\varepsilon_2 = 0.23$, $\gamma = 28^\circ$ inferred – by simultaneously matching the signature splitting behavior and B(E2) using the particle rotor model – was much higher than that for $^{129}$Cs ($\varepsilon_2 = 0.15$, $\gamma = 18^\circ$). We also observed a sudden increase in the B(E2) value at the inversion point which could be attributed to bandcrossing phenomenon, thereby changing the configuration from single quasi-particle to three-quasi particle. Further, a higher value of triaxiality parameter ($\gamma$) is expected above the bandcrossing. The decay scheme of $^{127}$I indicates a decoupling behavior, much pronounced than in $^{129}$Cs. In the Cranking model picture, $^{127}$I inverts from normal splitting to anomalous splitting at spin $19/2^+$. In future, it will be interesting and worthwhile to populate the highest possible spin states in $^{127}$I, to observe a possible flip from anomalous splitting to normal again due to another signature inversion.

### Acknowledgements

We wish to thank B. Kanagalekar, B. Bhujang and V. Pasi for participating in the experiment, and supporting during the initial part of data analysis. Special thanks to R. Palit, S. Muralithar, and R. P. Singh for their contribution in successful completion of the experiments. The full cooperation of the Pelletron staff at TIFR and IUAC is also thankfully acknowledged. This work is partly supported by the Department of Atomic Energy, Government of India (Project Identification Code: 12-R&D-TFR-5.02-0200), and the Department of Science and Technology, Government of India (Grant No. IR/S2/PF-03/2003-II).

## References

[1] T. Koike, K. Starosta, C.J. Chiara, D.B. Fossan, D.R. La Fosse (2003) *Phys. Rev.* **C 67** 044319-22. DOI: 10.1103/PhysRevC.67.044319.

[2] V. Kumar, P. Das *et al.* (2010) *Phys. Rev.* **C 82** 054302-07. DOI: 10.1103/PhysRevC.82.054302.

[3] K. Starosta, T. Koike *et al.* (2001) *Phys. Rev. Lett.* **86** 971-974. DOI: 10.1103/PhysRevLett.86.971.

[4] P. Das, H.K. Singh, U. Lamani, S. Muralithar, R.P. Singh (2020) *Acta Phys. Pol.* **B 51** 103-108. DOI: 10.5506/APhysPolB.51.103.

[5] Hartley *et al.* (2002) *Phys. Rev.* **C 65** 044329: 1-22. DOI: 10.1103/PhysRevC.65.044329.

[6] B. Kanagalekar, P. Das, B. Bhujang, S. Muralithar, R.P. Singh, R.K. Bhowmik (2013) *Phys. Rev.* **C 88** 054306: 1-15. DOI: 10.1103/PhysRevC.88.054306.

[7] H.K. Singh, P. Das, B. Kanagalekar, S. Muralithar, R.P. Singh (2019) *Phys. Rev.* **C 100** 064306: 1-10. DOI: 10.1103/PhysRevC.100.064306.

[8] U. Lamani, P. Das, B. Bhujang, V. Pasi (2021) *Nucl. Phys.* **A 1014** 122220: 1-16. DOI: 10.1016/j.nuclphysa.2021.122220.

[9] T.K. Alexander, J.S. Foster (1978) Lifetime Measurements of Excited Nuclear Levels by Doppler-Shift Methods. In: M. Baranger, E. Vogt (eds) "*Advances in Nuclear Physics, vol 10*". Plenum Press, New York, London, pp. 197—331.

[10] R. Palit *et al.* (2013) In: *J. Phys.: Conf. Ser.,* **420**, 012159. DOI: 10.1088/1742-6596/420/1/012159.

[11] S. Muralithar *et al.* (2011) Indian National Gamma Array at IUAC. In: *J. Phys.: Conf. Ser.,* **312**, 052015. DOI: 10.1088/1742-6596/312/5/052015.

[12] P. Petkov, D. Tonev, A. Dewald, P. von Brentano (2002) *Nucl. Instrum. Meth. Phys.* **A 488** 555–561. DOI: 10.1016/S0168-9002(02)00555-7.

[13] J.C. Wells, N.R. Johnson (1991) "*ORNL Report* **6689**". pp. 44.

[14] J. Srebrny, Ch. Droste *et al.* (2001) *Nucl. Phys.* **A 683** 21-47. DOI: 10.1016/S0375-9474(00)00457-7.

[15] S.E. Larsson, G. Leander, I. Ragnarsson (1978) *Nucl. Phys.* **A 307** 189-223. DOI: 10.1016/0375-9474(78)90613-9.

[16] I. Ragnarsson, private communication.

[17] D. Singh, A. Gupta, A. Kumar *et al.* (2021) *Nucl. Phys.* **A 952** 41-61. DOI: 10.1016/j.nuclphysa.2016.04.014.

[18] J.N. Orce, A.M. Bruce, A. Emmanouilidis *et al.* (2006) *Phys. Rev.* **C 74** 034318: 1-12. DOI: 10.1103/PhysRevC.74.034318.

[19] B. Ding, Y.H. Zhang, X.H. Zhou *et al.* (2012) *Phys. Rev.* **C 85** 044306: 1-14. DOI: 10.1103/PhysRevC.85.044306.

[20] S. Das, S. Samanta, R. Bhattacharjee, R. Raut *et al.* (2017) *Nucl. Instrum. Methods* **A 841** 17-23. DOI: 10.1016/j.nima.2016.10.022.

[21] R. F. Casten (1990) "*Nuclear structure from simple perspective*" (Oxford University press), pp. 280-290.